Numerical Simulation Study of Temperature Gradient Transient Liquid Phase Bonding with Concentration-Dependent Diffusivity

O.E. BAMIDELE and O.A. OJO

A new numerical model is developed to study the kinetics of temperature gradient transient liquid phase (TG-TLP) bonding under concentration-dependent diffusivity by using a first-order implicit–explicit finite-difference numerical method and Landau coordinate transformation with adaptable spatial discretization. The model is validated with experimental data reported in the literature. The results of computational analysis by the new model show that the presence of solute concentration gradient in the liquid is the major factor that enables shorter solidification completion time in TG-TLP bonding compared to the conventional transient liquid phase bonding (C-TLP bonding). In contrast to the common assumption that solid-state diffusion can be ignored during the modeling of TG-TLP bonding, this work shows that solid-state diffusion plays a significant role, not only in controlling the transition in solidification behavior from bidirectional to unidirectional, but also affects the kinetics of the bonding process. Moreover, it is found that the anomalous increase in solidification completion time with increase in temperature that occurs during C-TLP bonding can be avoided by TG-TLP bonding. This is possible if the solute concentration gradient in the liquid is sufficiently high to enable adequate solidification kinetics to overcome increased volume of liquid that accompanies increase in bonding temperature.

https://doi.org/10.1007/s11661-021-06219-3
© The Minerals, Metals & Materials Society and ASM International 2021

I. INTRODUCTION

TRANSIENT liquid phase (TLP) diffusion bonding was developed to avoid cracking problems encountered during the welding of difficult-to-weld advanced materials, such as nickel based superalloys that are used in aircraft gas turbine engines.[1–4] There are four main stages in the TLP bonding process: heating, base-metal dissolution, isothermal solidification, and homogenization.[5,6] When the TLP sample is heated to the joining temperature, a liquid layer forms between two adjoining solids. The melting point depressant (MPD) solute inside the liquid, which causes the melting of the filler alloy, subsequently diffuses into the solid substrate, thereby, producing isothermal solidification of the liquid phase. One of drawbacks of TLP bonding is that a substantial holding time is required to obtain complete isothermal solidification of the liquid.[7] If the holding time is insufficient, deleterious micro-constituents will be formed within the joint region from the residual liquid during cooling and degrade the properties of bonded materials.[8] Researchers such as Shirzadi and Wallach[1] and Yang *et al*.[9] have reported that the processing time during TLP bonding can be reduced by imposing temperature gradient across the bond line (TG-TLP bonding) compared to when the temperature is uniform, as in the case of conventional TLP bonding (C-TLP bonding). Similarly, studies carried out by Jabbareh and Assadi,[10] and Shirzadi and colleagues[11] on joint morphology show that TG-TLP bonding produces a more reliable and higher bond strength compared to C-TLP diffusion bonding. To take full advantage of TG-TLP bonding process, the mechanisms involved need to be adequately understood. Although various studies in the literature have indicated that TG-TLP bonding can produce a shorter bonding time compared to C-TLP bonding process, the main factor that enables the fast solidification behavior has not been adequately studied and explained. To elaborate, during TG-TLP bonding, only one solid–liquid interface undergoes solidification, whereas in C-TLP bonding, the two solid–liquid interfaces experience solidification. Also, during TG-TLP bonding, more liquid is produced into the joint region as the solidification progresses due to the melting that occurs at one of the two solid–liquid interfaces, whereas in C-TLP bonding, no extra liquid is

O.E. BAMIDELE and O.A. OJO are with the Department of Mechanical Engineering, The University of Manitoba, Winnipeg, MB, R3T 5V6, Canada. Contact e-mails: oluwasola68@gmail.com, olanrewaju.ojo@umanitoba.ca

Manuscript submitted September 2, 2020; accepted February 20, 2021.

Article published online April 3, 2021

produced once solidification starts. These two factors can be expected to increase the time required to achieve complete solidification during TG-TLP bonding, which is in contrast to what is generally reported in the literature that solidification completion time is shorter during TG-TLP bonding. Furthermore, reports in the literature on TG-TLP bonding discuss the effects of TG magnitude on the bonding process; however, the same magnitude of TG can occur over different ranges of temperature. The effect of variation in temperature range, for a given TG value, on the kinetics of the bonding process is not generally discussed in the literature. Therefore, the two major goals of the present work are to develop a diffusion-based numerical model to systematically study and understand the key factor that enables TG-TLP bonding to be faster than C-TLP bonding and analyze the influence of variation in temperature range, for a given TG, on the solidification kinetics. Most of the existing TG-TLP bonding models in the literature assume that the solute diffusion coefficient in the solid substrates is independent on solute concentration. It is known, however, that solid-state diffusion coefficient can significantly vary with solute concentration. Therefore, to properly address the two key objectives of the present work, the numerical model developed in this work incorporates concentration-dependent diffusion coefficient. The development of the new numerical model and the results of the study are presented and discussed in this article.

II. DEVELOPMENT OF THE NUMERICAL MODEL AND VALIDATION

A. *Governing Equations*

The numerical model for the TG-TLP bonding problem is based on Fick's second law of diffusion. In this research, planar geometry is used. The two moving solid–liquid interfaces can be modeled with a velocity term known as Stefan's equation.

The main assumptions in the model development are

1. The geometry of the solid–liquid interfaces remains planar throughout the bonding process.
2. Local equilibrium exists at the solid–liquid interface so that the liquidus and the solidus concentrations are derived from the liquidus and the solidus lines in the binary equilibrium phase diagram.
3. The liquidus and the solidus lines are assumed linear with constant slopes.
4. Variations of temperature with solute concentration is constant (*i.e.*, $\mathrm{d}T/\mathrm{d}C = K$).
5. Temperature gradient across the TLP bonding assembly is linear.
6. The molar volumes of the phases involved are assumed constant.
7. Change of the liquid composition has no effect on the liquid diffusion coefficient.

The equations required to model the diffusion problem in a three-phase binary system are shown as Eqs. [1] through [4]. Equation [1] describes the diffusion of the solute in the first solid phase (Base Metal A), Eq. [2] for the liquid phase (Filler alloy B), and Eq. [3] for the second solid phase (Base Metal C). Equation [4] is the velocity term that describes the movement of the first solid–liquid interface (Interface 1) and Eq. [5] is for the second solid–liquid interface (Interface 2), where C is the composition profile of the solute in each of the phases expressed as a function of position (x) and time (t). $D_{\mathrm{A,C}}(x,)$ and $D_{\mathrm{B}}(x,)$ are the diffusion coefficients of the two solids and liquid, respectively. $C_{\mathrm{BA}}, C_{\mathrm{BC}}$, C_{CB} , and C_{AB} are the equilibrium liquidus and solidus composition values for the phases.

$$\frac{\partial C(x,t)}{\partial t} = \frac{\partial}{\partial x}\left[D_{\mathrm{A}}(c)\frac{\partial C(x,t)}{\partial x}\right], \quad [1]$$

$$\frac{\partial C(x,t)}{\partial t} = \frac{\partial}{\partial x}\left[D_{\mathrm{B}}(c)\frac{\partial C(x,t)}{\partial x}\right], \quad [2]$$

$$\frac{\partial C(x,t)}{\partial t} = \frac{\partial}{\partial x}\left[D_{\mathrm{C}}(c)\frac{\partial C(x,t)}{\partial x}\right], \quad [3]$$

$$[C_{\mathrm{BA}} - C_{\mathrm{AB}}]\frac{\mathrm{d}s1}{\mathrm{d}t} = D_{\mathrm{A}}\frac{\partial C(x,t)}{\partial x}\Big|_{x=s1^-} - D_{\mathrm{B}}\frac{\partial C(x,t)}{\partial x}\Big|_{x=s1^+}, \quad [4]$$

$$[C_{\mathrm{BC}} - C_{\mathrm{CB}}]\frac{\mathrm{d}s2}{\mathrm{d}t} = D_{\mathrm{C}}\frac{\partial C(x,t)}{\partial x}\Big|_{x=s2^-} - D_{\mathrm{B}}\frac{\partial C(x,t)}{\partial x}\Big|_{x=s2^+}. \quad [5]$$

To achieve solute conservation, the concept of Landau transformation technique that was first introduced by Illingworth *et al.*[12] is used in the present work. It is worth noting that in this TG-TLP bonding model, the solute diffusion coefficients in the liquid and solid phases are not constant throughout the bonding process as in the case of the C-TLP bonding process. Instead, the diffusion coefficients vary with temperature based on the Arrhenius equation [6]. Moreover, the diffusion coefficient in the solid also varies with solute concentration, so it will be modeled with the concentration-dependent relation used by Ghanbar *et al.*,[13] as shown in Eq. [7].

$$D(T) = D_0\exp\left(\frac{-Q}{R(T_0 + GX)}\right), \quad [6]$$

$$D(T,C) = D_0\exp\left(\frac{-Q}{R(T_0 + GX)}\right).\exp(k(C - C_{\mathrm{o}})). \quad [7]$$

B. *Spatial Discretization of Governing Equations*

Landau transformation can be used to obtain new coordinates in which the grids are fixed, but space meshing automatically adjusts to accommodate the motion of a migrating interface.[14] New positioning variables $u = \frac{x}{s1(t)}$, $w = \frac{x-s1}{s2(t)-s1(t)}$, and $v = \frac{x-s2(t)}{L-s2(t)}$ are introduced such that the coordinate ranges from $0 < u < 1$ for phase A, $0 < w < 1$ for phase B, and $0 < v < 1$ for phase C, respectively. Obtaining transformed expressions for each concentration profile will need the application of some mathematical procedures. The expressions obtained from the transformation analysis in each phase are given in Figure 1.

1. *Implicit–explicit scheme*

A numerical approach that can be used for any particular diffusion problem strongly depends on the value of the diffusion coefficient, initial interface conditions, and desired accuracy. In a system where diffusivity does not significantly depend on the solute concentration, for example in liquid-state diffusion, a typical implicit up/downwind approach provides the most stable solution.[12] However, if the diffusivity is concentration-dependent, like in the solid-state diffusion, the use of an explicit scheme for the solution of the diffusion term and up/downwind scheme for the convective term would provide a more stable solution.[15] In the present work, an hybrid approach is used. Implicit method is used for the diffusion analysis in the liquid phase and explicit scheme is used for solid-state diffusion.

The numerically integration for each Eqs. [8], [9], and [10] follows finite volume technique[16] with the spatial coordinates discretized with equal spatial division. Hence, the finite-difference approximation solutions for each of the phases are listed below, while further solutions are shown in Appendix.

2. *Phase A*

$$\frac{\left\{p_j^{n+1} s1^{n+1} - p_j^n s1^n\right\}}{\Delta t} = \frac{\left\{s1^{n+1} - s1^n\right\}}{\Delta t} \frac{p_{j+1/2}^n u_{j+1/2} - p_{j-1/2}^n u_{j-1/2}}{\Delta u^e} + \frac{1}{s1^n(t).\Delta u^2} \left\{(D_A)_{j+\frac{1}{2}}^n p_{j+1}^n + (D_A)_{j-\frac{1}{2}}^n p_{j-1}^n - \left[(D_A)_{j+\frac{1}{2}}^n + (D_A)_{j-\frac{1}{2}}^n\right] p_j^n\right\}. \quad [8]$$

3. *Phase B*

$$\frac{z_j^{n+1}\left(s2^{n+1} - s1^{n+1}\right) - z_j^n\left(s2^n - s1^n\right)}{\Delta t} = \frac{\left(s1^{n+1} - s1^n\right)}{\Delta t} \frac{z_{j+1/2}^{n+1} - z_{j-1/2}^{n+1}}{\Delta w^e} + \frac{s2^{n+1} - s1^{n+1} - s2^n + s1^n}{\Delta t} \frac{z_{j+1/2}^{n+1} w_{j+1/2} - z_{j-1/2}^{n+1} w_{j-1/2}}{\Delta w^e} + \frac{1}{\Delta w^2\left(s2^{n+1} - s1^{n+1}\right)} \left\{(D_B)_{j+\frac{1}{2}}^{n+1} z_{j+1}^{n+1} + (D_B)_{j-\frac{1}{2}}^{n+1} z_{j-1}^{n+1} - \left[(D_B)_{j+\frac{1}{2}}^{n+1} + (D_B)_{j-\frac{1}{2}}^{n+1}\right] z_j^{n+1}\right\}. \quad [9]$$

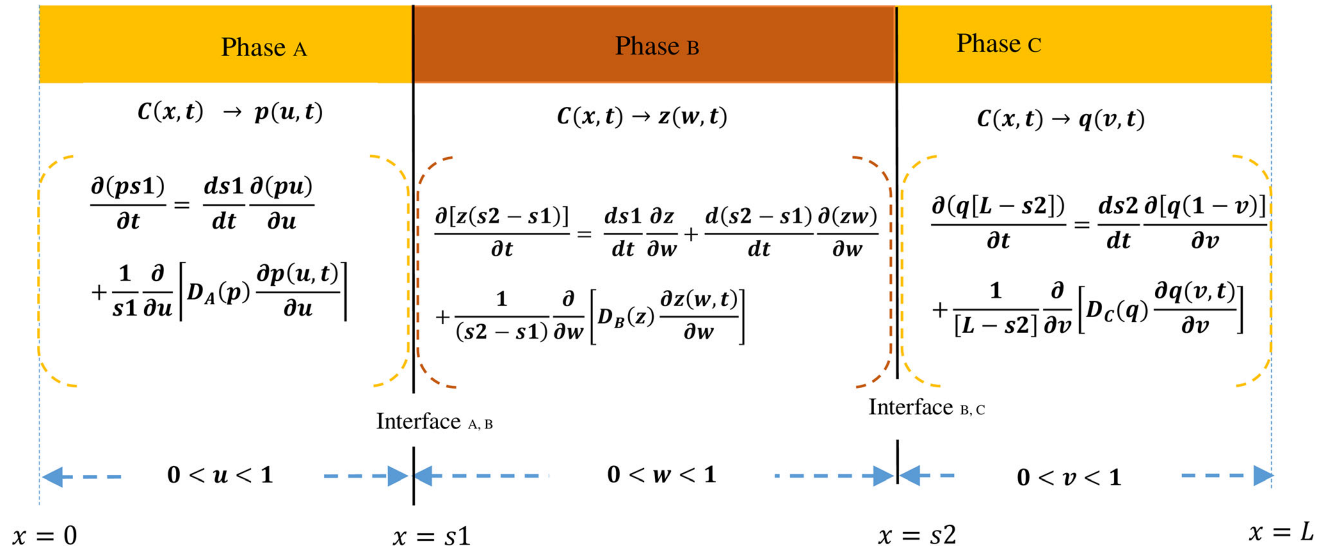

Fig. 1—Illustration of the new TG-TLP bonding model scheme based on Landau transformation with moving boundary interfaces.

4. *Phase C*

$$\frac{\left\{q_j^{n+1}\left(L - s2^{n+1}\right) - q_j^n\left(L - s2^n\right)\right\}}{\Delta t} = \frac{\left\{s2^{n+1} - s2^n\right\}}{\Delta t}\frac{q_{j+1/2}^n\left(1 - v_{j+1/2}\right) - q_{j-1/2}^n\left(1 - v_{j-1/2}\right)}{\Delta v^e} + \frac{1}{\Delta v^2[L - s2^n]} \left\{(D_\mathrm{C})_{j+\frac{1}{2}}^n q_{j+1}^n + (D_\mathrm{C})_{j-\frac{1}{2}}^n q_{j-1}^n - \left[(D_\mathrm{C})_{j+\frac{1}{2}}^n + (D_\mathrm{C})_{j-\frac{1}{2}}^n\right] q_j^n\right\}, \quad [10]$$

where $(D_\mathrm{A})_{j+1/2}^n$ corresponds to the diffusion coefficient for the solute concentration that is halfway between the discretized points $(j+1)$ and (j), while $(D_\mathrm{A})_{j-1/2}^n$ corresponds to the diffusion coefficient for the solute concentration halfway between (j) and $(j-1)$.

C. *Implementation*

Figure 2 shows the spatial mesh of the three mass transfer domains considered. The initial and the boundary conditions of these domains can be written as follows:

$$\forall t \geq 0, \quad \frac{\partial p}{\partial u} = \frac{\partial q}{\partial v} = \begin{cases} 0, & u = 0, \\ 0, & v = 1. \end{cases} \quad [11]$$

This means that no mass transfer is allowed beyond the boundaries of the system. In addition, the boundary conditions at the interfaces are as follows:

$$t \geq 0, \quad C(x,t) = \begin{cases} C_\mathrm{AB}^n, & x = s_1^-, \\ C_\mathrm{BA}^n, & x = s_1^+, \\ C_\mathrm{BC}^n, & x = s_2^-, \\ C_\mathrm{CB}^n, & x = s_2^+. \end{cases} \quad [12]$$

The interface equilibrium concentrations C_AB^n,C_BA^n, C_BC^n , and C_CB^n change with temperature along the TG line, and are modeled by using Eqs. [A3] through [A6] listed in the Appendix with the assumption that the interface compositions are changing linearly with temperature, which is denoted with ‘m.’ Likewise, the TG across the liquid width is linear. The parameter ‘f’ in the expressions serves as an equilibrium partitioning coefficient between the liquidus and the solidus lines.

D. *Moving Boundary Equations*

The two moving solid/liquid interfaces can be tracked by discretizing the interface equations [4] and [5] with the requirement that solute is conserved at each interface or by an alternative form derived from the finite-difference approximation solution of the phases through the substitution of boundary conditions at each interface.

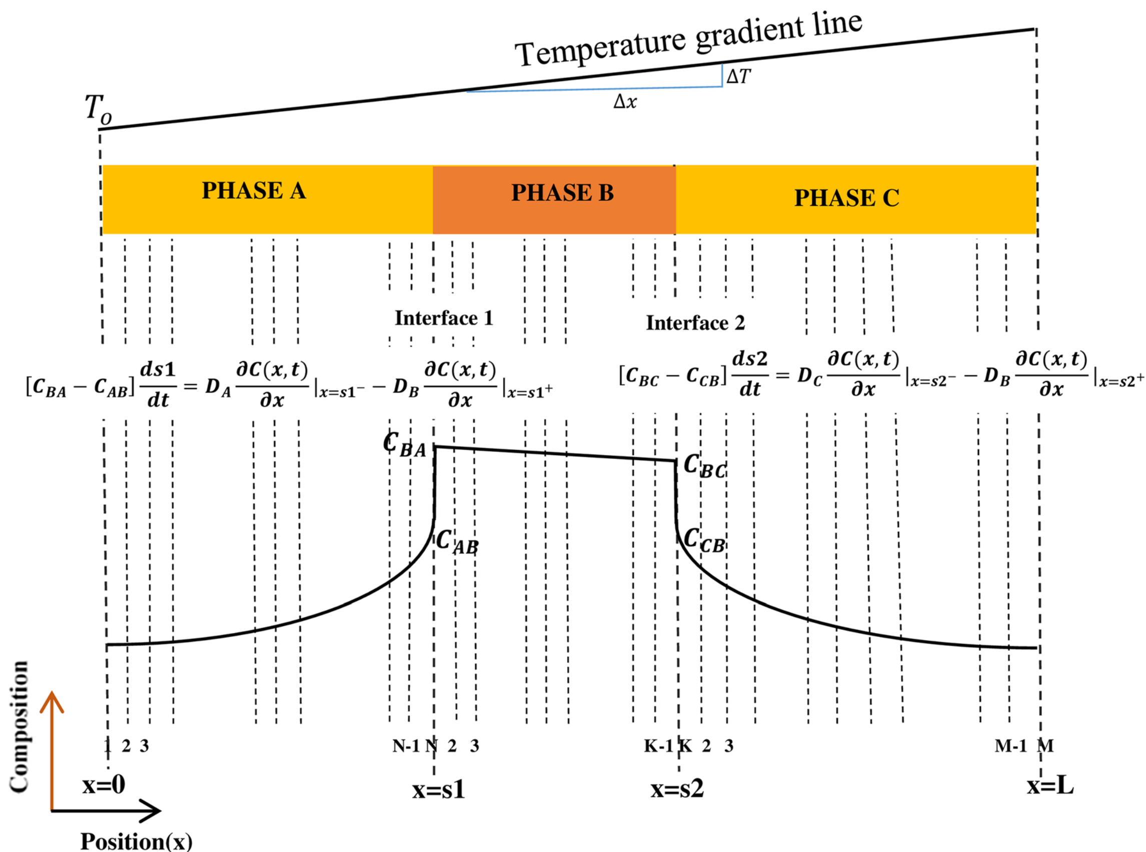

Fig. 2—Illustration of discretization of spatial coordinates [0, 1] of u, w, and v in phases A to C.

Interface 1:

$$s1^{n+1} = s1^n + \Delta t \cdot \left(\frac{(D_B)^n_{1/2}}{(s2^n - s1^n)} \frac{(z^n_2 - C^n_{BA})}{w_2} - \frac{(D_A)^n_{N-1/2}}{s1^n} \frac{(p^n_{N-1} - C^n_{AB})}{(1 - u_{N-1})} \right) / (C^n_{AB}(1 - u_{N-1/2}) + p^n_{N-1/2} u_{N-1/2} - C^n_{BA} w_{1/2} - z^n_{1/2}(1 - w_{1/2})) \quad [13]$$

interface 2:

$$s2^{n+1} = s2^n + \Delta t \cdot \left(\frac{(D_C)^n_{\frac{1}{2}}(q^n_2 - C^n_{CB})}{v_2[L - s2^n]} - \frac{(D_B)^n_{K-\frac{1}{2}}(z^n_{K-1} - C^n_{BC})}{(1 - w_{K-1})[s2^n - s1^n]} \right) / (C^n_{BC}(1 - w_{K-1/2}) + z^n_{K-1/2} w_{K-1/2} - C^n_{CB} v_{1/2} - q^n_2(1 - v_{1/2})). \quad [14]$$

A computational program code is developed to implement the following algorithm, which, at each time step, carries out the following steps:

1. s^n is used as the initial interface position in order to determine the future interface position s^{n+1}, as it applies to both interfaces.
2. p^n_j, z^n_j, and q^n_j represent the solute concentration in profiles p, z, and q at the initial bonding time n.
3. The future interface positions $s1^{n+1}$ and $s2^{n+1}$ are determined by using the interface solutions calculated with Eqs. [13] and [14], respectively.
4. The future solute concentration profiles p^{n+1}_j, q^{n+1}_j, and z^{n+1}_j are updated by using the finite-difference approximation solution of each phase and the new interface positions $s1^{n+1}$ and $s2^{n+1}$.
5. The value of s^n, p^n_j, z^n_j, and q^n_j is replaced with s^{n+1}, p^{n+1}_j, z^{n+1}_j, and q^{n+1}_j, respectively.
6. The current s^n, p^n_j, z^n_j, and q^n_j in Step 5 is used to produce the new future interface position and future solute concentration profiles.
7. Steps 3 to 6 are repeated multiple times until the gap between the two moving interfaces reaches the set space limit. Then, the algorithm will break, which signifies the end of the solidification process.

E. *Validation of the New Model*

Using a Bi-Sn binary system and process parameters listed in Table I, spatial convergence tests were performed by varying a mesh density that carried from 50 to 1000 elements. The predicted interface position with time was found to be dependent on spatial discretization as the mesh density was increased, as shown in Figure 3. However, increasing the spatial resolution to over 400 points/mm was found to have less effect on the accuracy of the solution. The results show that a truncation error caused by the use of a 400 points/mm space-step resulted in a predicted interface location that is 1.3 μm off of the converged solution, which shows that the error in the model solution is considered minimal. Time discretization tests were also performed by varying time step from 0.5 to 50 ms. Figure 4 shows that the predicted interface position is also dependent of the time discretization as the time step size was decreased. The truncation error caused by the use of a coarse time step of 50 ms resulted

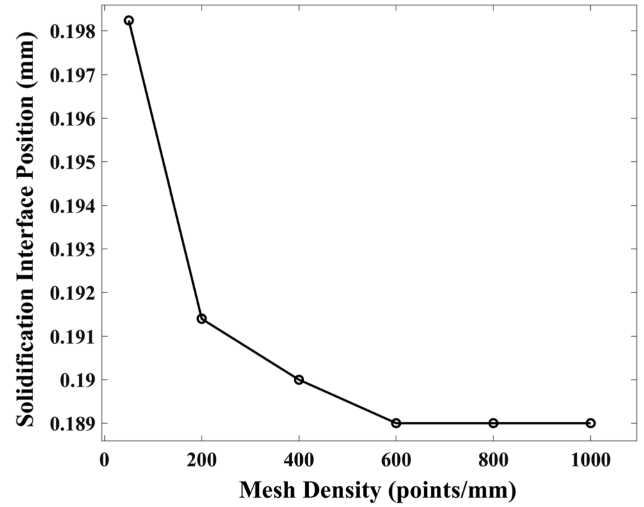

Fig. 3—Effect of mesh density on predicted interface position at TG of 50°C/cm, gap size 50 μm.

Table I. Processing Parameters Used for Numerical Simulation of TG-TLP Bonding

Parameter	Symbol	Value
Binary System	—	Sn-Bi
Diffusion Coeff. of Bi in Liquid Sn $D = D_L \times \exp(Q_L/RT)$	mm^2/s	$D_L = 2.934\,2 \times 10^{-2}$
	kJ/mol	$Q_L = 12.16$[17]
Diffusion Coefficient of Bi in Solid Sn $D = D_s \times \exp(Q_s/RT)$	mm^2/s	$D_s = 1.18 \times 10^5$
	kJ/mol	$Q_s = 99.72$[18]
Lowest Temperature T_o	°C	150
Initial Bi Composition in Liquid Sn	at. pct	43
Initial Bi Composition in Solid Sn	at. pct	0
Conc. Dependency Diffusivity Constant k		− 0.1
Base-Metal Thickness	μm	1000

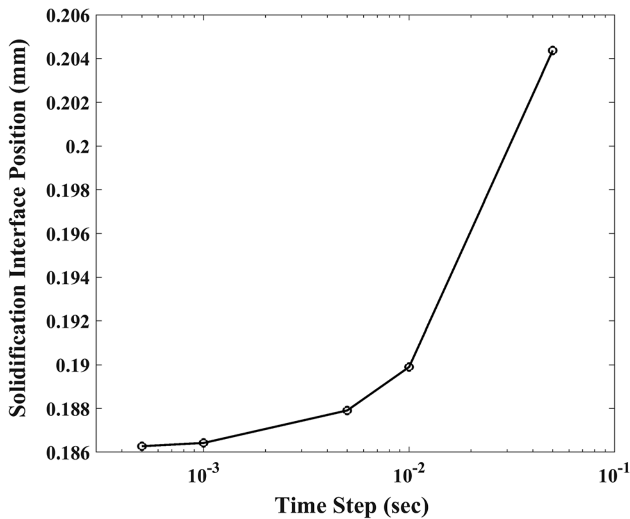

Fig. 4—Effect of time steps on predicted interface position at TG of 50°C/cm, gap size 50 μm.

in a predicted interface location that is 18μm off of the converged solution.

The newly developed model is versatile such that apart from TG-TLP bonding, it can also be used to simulate C-TLP bonding process. To initially validate the new model, simulation of C-TLP bonding was performed at a constant temperature for a single-crystal nickel alloy (base metal) with a thickness of 3000 μm and a filler alloy with a half thickness of 12.5 μm, which are similar to the specifications used in Zhou *et al.*[5] and Illingworth *et al.*[12] A comparison of the results of the new model with those in Zhou *et al.*[5] and Illingworth *et al.*[12] by using the same initial and boundary conditions (listed in Table II) is shown in Figure 5. In addition, the model results are compared with the experimental data for C-TLP bonding of nickel as reported by Zhou *et al.*[5] The movement of the two interfaces in this symmetrical system as predicted by the present model is found to be comparable with the result of a previous numerical analysis[12] and experimental data.[5] Also, the maximum dissolution width of the liquid does not exceed the theoretical maximum value of 23.2 μm which indicates that the model conserves the solute.

Aside from validating the model with C-TLP bonding, the newly developed numerical model is used to examine how the solidification distance changes with time during the TG-TLP bonding process for a tin-bismuth alloy, and the results are presented in Figure 6. The results show that the velocity of the solidification is not constant but reduces with time. Based on the results of the model presented in Figure 6, the relationship between the solidification distance and bonding time can be represented with a general equation as follows:

$$Y = \alpha t^n, \quad [15]$$

where α is a constant parameter at a given temperature and n is a time index value. Using the logarithmic form of Eq. [15] yields Eq. [16]. Based on Eq. [16], a straight line is expected if $\log Y$ is plotted against $\log t$. The slope of the straight line will give the exponent n, and the intercept of the line on the vertical axis (log Y axis) produces the constant α.

$$\log Y = n \log t + \log \alpha. \quad [16]$$

Some data are extracted from Figure 6 and used to plot the log of the solidification distance against the log of time. The results are shown in Figure 7. The results show that a log–log plot of the solidification distance *vs.* time results in a straight line with a slope that is greater than 0.5 (the time index in C-TLP bonding, obtained by removing the temperature gradient and making the temperature constant). Therefore, the new model indicates that during TG-TLP bonding, a log–log plot of the solidification distance against holding time will produce a linear relationship and the slope of the linear plot will be larger than 0.5. In order to validate these predictions from the newly developed model, some TG-TLP bonding experimental data are obtained from Zhong *et al.*[19] and Yin *et al.*,[20] and the log of the solidification distance is plotted against the log of time. The results are presented in Figure 8. The two different sets of experimental data show that the relationship between the log–log plot of the solidification distance and time is a straight line. Also, the slope of the straight line is consistently higher than 0.5, which agrees with the prediction of the new model. Therefore, the experimental results are in qualitative agreement with the predictions of the newly developed model. In addition, another qualitative validation of the model prediction was performed. The new model predicts that apart from the unidirectional solidification that is reported in the literature to occur during TG-TLP bonding, it is possible to first have a bidirectional solidification, which can subsequently translate to unidirectional solidification, under a low-temperature gradient condition (Figure 9). The results of an experimental work performed by Bigvand[21] show that during TG-TLP bonding, the solidification process started with bidirectional solidification mode and later changed to unidirectional solidification, which concurs with the prediction of the newly developed model in this work.

III. RESULTS AND DISCUSSION

A. *Investigation of the Key Factor that Enables Shorter Solidification Completion Time During TG-TLP Bonding Compared to C-TLP Bonding*

Time is a crucial parameter in TLP bonding that affects the microstructure of the bonded joint. If sufficient time is not used to enable complete solidification of the liquid, the residual liquid will solidify during cooling to produce non-equilibrium solidification products that can be deleterious to the mechanical properties of the joint. It has been suggested in the literature that one of the advantages of TG-TLP bonding process over C-TLP bonding process is its ability to reduce solidification completion time t_f.[9,19] Nevertheless, it is important to identify the exact factor that is responsible for

Table II. Processing Parameters Used in Experimental Data and Numerical Predictions for C-TLP bonding in Zhou *et al.*[5] and Illingworth *et al.*[12]

Parameter	Symbol	Value
Materials Data		
Binary System	—	nickel-phosphorus (Ni-P)
Diffusion Coeff. of P in Liquid Ni	$\mu m^2/s$	500
Diffusion Coefficient of P in Solid Ni	$\mu m^2/s$	18
Initial Conditions		
Composition of P in Filler Alloy	at. pct	19
Composition of P in Base Metal	at. pct	0
Boundary Conditions		
Bonding Temperature	°C	1150
Liquidus Composition	at. pct	10.223
Solidus Composition	at. pct	0.166
Model Parameters		
Filler Half Thickness	μm	12.5
Base Thickness	μm	3000

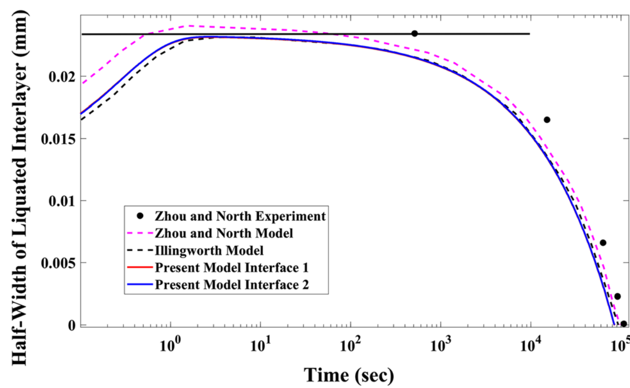

Fig. 5—Plot of movement of two solid/liquid interface in Ni-P binary alloy system based on Zhou *et al.*[5] and Illingworth *et al.*[12]

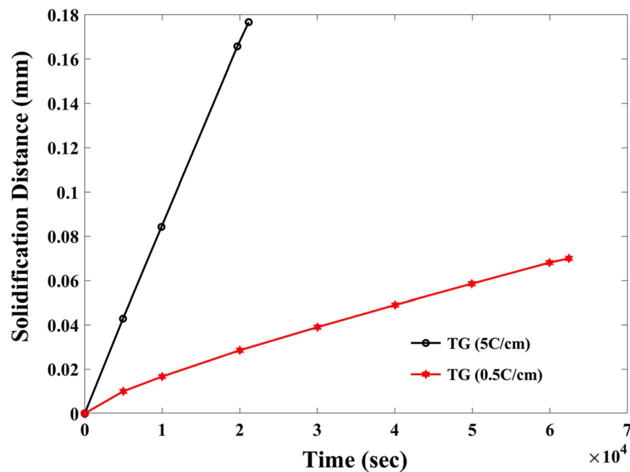

Fig. 6—Movement of the solidifying interface *vs.* time during TG-TLP bonding for tin-bismuth alloy.

reducing the t_f. In order to appropriately compare the two bonding methods, there is a need to determine the proper bonding temperatures to use because bonding during the C-TLP occurs at a constant temperature,

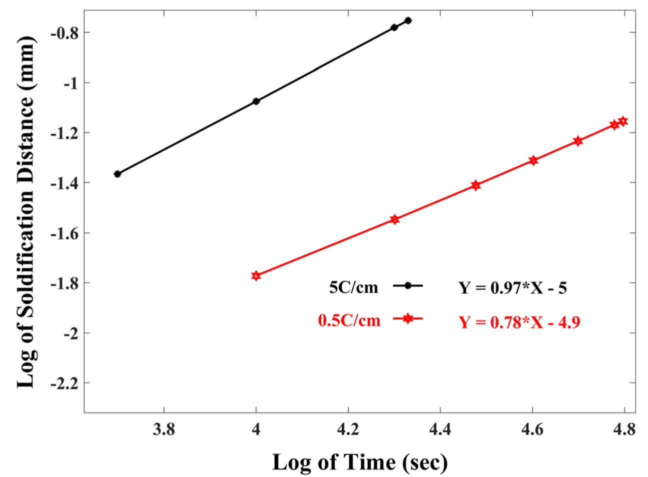

Fig. 7—Log–log plot of solidification distance *vs.* time with data from Fig. 6.

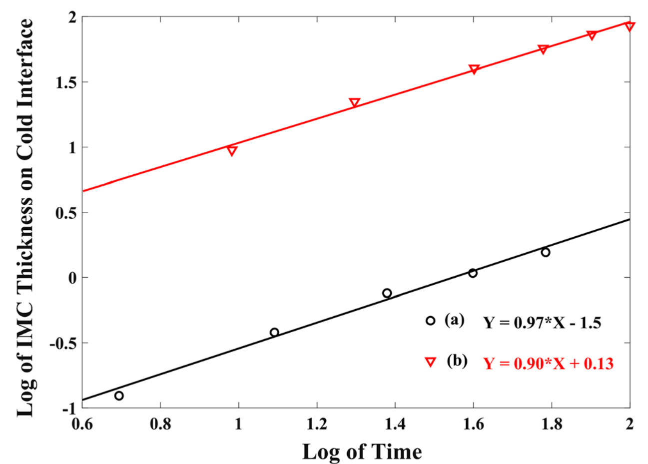

Fig. 8—Plot of log of intermetallic compound growth on cold interface against log of time in TG-TLP bonding process: (a) growth of Cu_6Sn_5,[20] and (b) growth of Ni_3Sn_4[19]

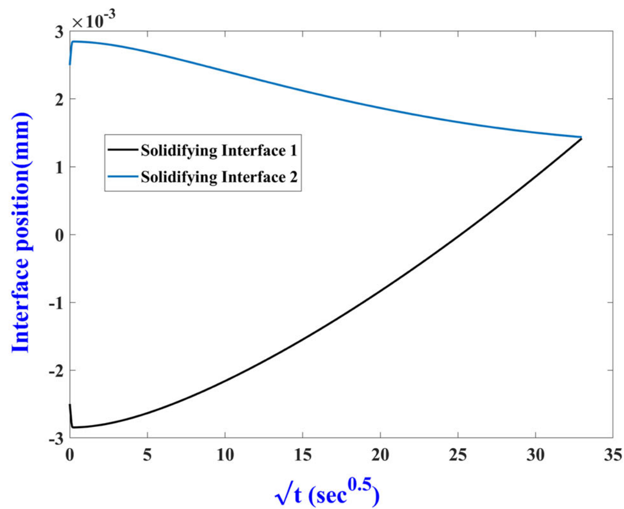

(a)

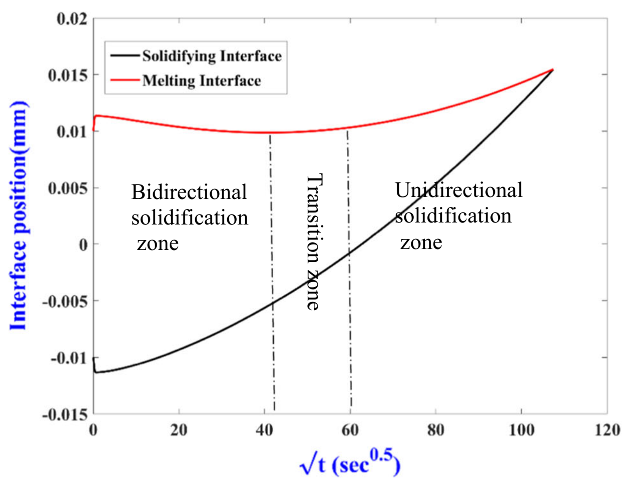

(b)

Fig. 9—Plot of interface displacement against $\sqrt{t}$; simulations performed with different gap sizes of (*a*) 5 μm, and (*b*) 20 μm under constant temperature gradient of 1 °C/cm. Parameters used are defined in Table I.

while bonding during the TG-TLP occurs over a range of different temperatures. A conservative approach is used in this study to compare these two bonding methods. TG-TLP bonding simulation is performed over a temperature range of 150 °C to 170 °C, and C-TLP bonding simulation is done at a constant temperature of 170 °C. Based on this approach, if the TG-TLP bonding process results in a shorter t_f relative to C-TLP bonding, then it confirms that TG-TLP bonding inherently has capability to shorten solidification completion time compared to C-TLP bonding. The reason is that higher temperature generally enhances solidification kinetics, which tends to reduce t_f. Since C-TLP bonding is done at a higher temperature, it is expected that its solidification kinetics would be faster and enables a shorter t_f. However, if the TG-TLP bonding, which is simulated at a lower overall temperature compared to the C-TLP bonding, produces

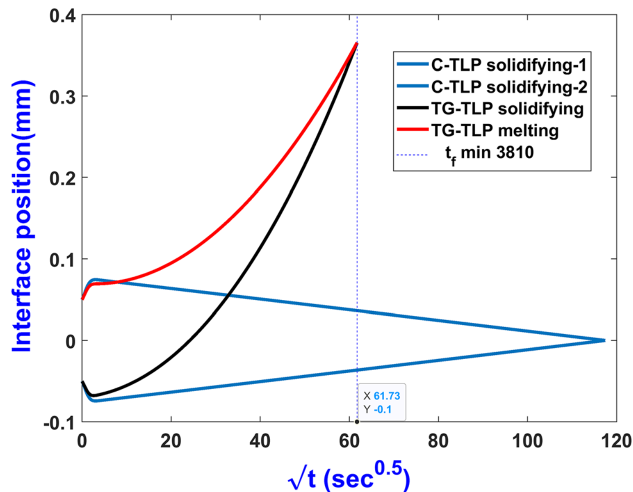

Fig. 10—Comparison of the bonding time between TG-TLP and C-TLP bonding under a TG of 50 °C/*cm*; maximum bonding temperature 170 °C; gap size 0.1 mm.

shorter t_f, the reason cannot be attributed to temperature effect, but must be an inherent characteristic of the TG-TLP bonding process. The results of the simulations of TG-TLP and C-TLP under the stated temperature conditions are presented in Figure 10. The results show that the TG-TLP bonding process produced a shorter t_f relative to the C-TLP bonding process, notwithstanding some opposing factors in the TG-TLP bonding. First, the TG-TLP bonding is done at a lower temperature while C-TLP bonding at a higher temperature. Secondly, in C-TLP bonding, the two solid–liquid interfaces undergo solidification, but in TG-TLP bonding, only one interface solidifies. Lastly, there is no production of extra liquid in C-TLP bonding during the solidification process, but in TG-TLP bonding, when one of the interfaces is solidifying, the other interface is melting.

To determine the key factor that enables the TG-TLP bonding method to produce the shorter t_f, a careful study was done by analyzing the mass balance equation that governs the migration velocity of the solid–liquid interface that undergoes solidification during the TG-TLP bonding process, as follows:

$$\frac{\mathrm{d}s1}{\mathrm{d}t} = \frac{1}{[C_{\mathrm{LA}} - C_{\mathrm{AL}}]}\left[D_{\mathrm{A}}\frac{\partial C}{\partial x_{\mathrm{s}}} - D_{\mathrm{L}}\frac{\partial C}{\partial x_{\mathrm{L}}}\right]. \qquad [17]$$

Based on Eq. [17], it is found that four parameters: D_{A}, D_{L}, $\frac{\partial C}{\partial x_{\mathrm{s}}}$, and $1/[C_{\mathrm{LA}} - C_{\mathrm{AL}}]$ have higher values in C-TLP bonding compared to TG-TLP bonding, due to the higher temperature in C-TLP bonding. The higher values of all these parameters facilitate the solidification process in C-TLP bonding relative to the TG-TLP. The only parameter that is higher in the TG-TLP bonding process and makes it to have a shorter t_f is the concentration gradient in the liquid phase $\left(\frac{\partial C}{\partial x_{\mathrm{L}}}\right)$. The value of this parameter is practically zero in the C-TLP bonding process because during isothermal solidification, the liquidus solute concentration on the two solid–liquid interfaces is the same. Therefore, no

concentration gradient across the liquid phase during the isothermal solidification stage. However, the liquidus solute concentration on both interfaces is different in TG-TLP bonding, because the two interfaces have different temperatures, which induces a concentration gradient across the liquid phase. Hence, this indicates that the major driving force which enables the TG-TLP bonding to exhibit a shorter t_f compared to the C-TLP is the occurrence of concentration gradient across the liquid phase, during the solidification process.

It has been recognized in the literature that diffusion through the liquid is responsible for shorter t_f during TG-TLP bonding compared to C-TLP bonding. Nevertheless, there are two components that control solute flux during liquid-state diffusion: the solute diffusivity and the concentration gradient. The analysis performed in this work has clearly showed that the solute concentration gradient in the liquid phase is the key factor that enables shorter t_f in TG-TLP bonding compared to C-TLP bonding. Notwithstanding that the influence of liquid-state diffusion, it is worthwhile to also analyze the role that solute diffusivity in the solid (D_s) plays during the TG-TLP bonding method. Generally, D_L is orders of magnitude higher than D_s. Accordingly, it has been assumed in the literature that solid-state diffusion can be ignored during the modeling of TG-TLP bonding, due to the low value of D_s relative to D_L and that the contribution of D_s to the whole process kinetics can be considered negligible.[1] However, calculations performed in this work show that an increase in the value of D_s can significantly reduce the solidification completion time t_f during TG-TLP bonding (Figure 11). The analysis in Figure 11 is performed at a constant temperature range and temperature gradient. The frequency factor and activation energy of D_L are kept

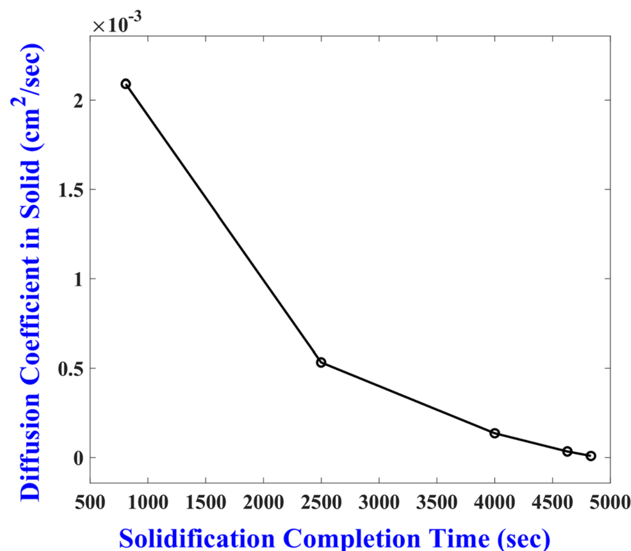

Fig. 11—Effect of increasing D_s on solidification completion time t_f (frequency factor and activation energy of D_L are kept constant, frequency factor of D_s is also kept constant, but the activation energy of D_s is varied) during TG-TLP bonding with temperature gradient of 50 °C/cm and a minimum temperature of 150 °C, and gap size of 0.1 mm.

constant, frequency factor of D_s is also kept constant, while the activation energy of D_s is varied. To explain the influence of D_s on the kinetics of TG-TLP bonding, it is vital to examine how the movement of the two solid–liquid interfaces changes with time during the solidification process. Also, it is worth noting that during the solidification process, the solute diffusivity in both the liquid and solid phases increases with increases in temperature along the TG direction. To simplify the analysis, all the values of frequency factor and activation energy for both the D_L and D_s are kept constant. The D_L and D_s only change as the temperature changes during the TG-TLP bonding process. The effects of the increase in the D_L and D_s with increases in temperature, during the process, are used to determine how D_L and D_s affect the kinetics of the bonding process. The kinetics as defined here are the slopes of the plot of the two solid–liquid interface displacements against the square root of time. The slope of the solidifying interface displacement is denoted as Φ_s, while that of the melting interface is Φ_m. Three cases are simulated. Case 1 is when the D_L and D_s values are kept constant with respect to the temperature, throughout the bonding process. This serves as the baseline condition for comparison purposes. Case 2 is when D_L increases with increases in temperature (denoted as $D_L^{\uparrow}$), and D_s is kept constant throughout the bonding process (denoted as D_s^*). This case is used to study the effect of D_L on Φ_m and Φ_s. Case 3 is when D_L is kept constant throughout the bonding process (denoted as D_L^*), and D_s increases with increases in temperature (denoted as $D_s^{\uparrow}$). This case is used to study the effect of D_s on Φ_m and Φ_s. The results of these simulations are presented in Table III. The results of Cases 1 and 2 show that increasing the value of D_L increases both Φ_s and Φ_m. However, increasing the value of D_s increases the Φ_s but decreases Φ_m. The extent of change in the Φ_m and Φ_s depends on the magnitudes of D_L and D_s used in the bonding process. It should be noted that to reduce the time t_f necessary to complete the bonding process and have all the liquid within the joint fully solidified, it is not only necessary for Φ_s to increase but it is also beneficial for Φ_m to reduce.

Accordingly, one of the reasons why a higher value of D_s contributes to a shorter solidification completion time t_f as shown in Figure 11 is because of the strong influence of D_s in decreasing Φ_m, which helps to reduce the extent of melting at the higher temperature solid–liquid interface during bonding. These results show that D_s can play a significant role during TG-TLP bonding, which may not be intuitively obvious. To clarify, when comparing C-TLP bonding to TG-TLP bonding, the major reason why solidification completion time is shorter in TG-TLP bonding relative to C-TLP bonding is due to the occurrence of concentration gradient across the liquid phase during TG-TLP bonding process, which is not present during C-TLP bonding. However, when just considering TG-TLP alone, the solidification completion time during TG-TLP bonding can be further reduced if the diffusion coefficient in the solid state, D_s, is increased. Moreover, analysis in this work shows that aside from the influence of D_s in aiding reduction in t_f,

Table III. Results of Three Hypothetical Cases of TG-TLP Bonding

$\sqrt{t}$	Case 1: D_L^*, D_s^* Φ_m	Φ_s	Case 2: $D_L^\uparrow, D_s^*$ Φ_m	Φ_s	Case 3: $D_L^*, D_s^\uparrow$ Φ_m	Φ_s
5	-4.1×10^{-4}	1.8×10^{-3}	-3.8×10^{-4}	1.9×10^{-3}	-6.5×10^{-4}	2.0×10^{-3}
15	9.9×10^{-4}	3.3×10^{-3}	1.1×10^{-3}	3.4×10^{-3}	7.6×10^{-4}	3.5×10^{-3}
30	3.1×10^{-3}	5.6×10^{-3}	3.3×10^{-3}	5.8×10^{-3}	2.8×10^{-3}	5.8×10^{-3}
45	5.1×10^{-3}	8.1×10^{-3}	5.4×10^{-3}	8.4×10^{-3}	—	—

Note: temperature gradient: 50°C/cm; gap size: 0.10mm, minimum temperature: 150 °C, and $D_s \approx 5.33x10^{-4}$cm^2/s.

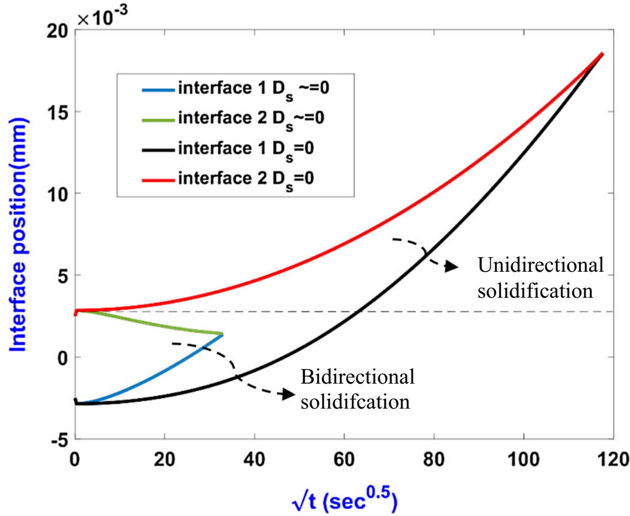

Fig. 12—Effects of solid-state diffusion (D_s) on direction of solidification during TG-TLP bonding process. $D_s \sim= 0$ (solid diffusion considered); $D_s = 0$ (solid diffusion neglected).

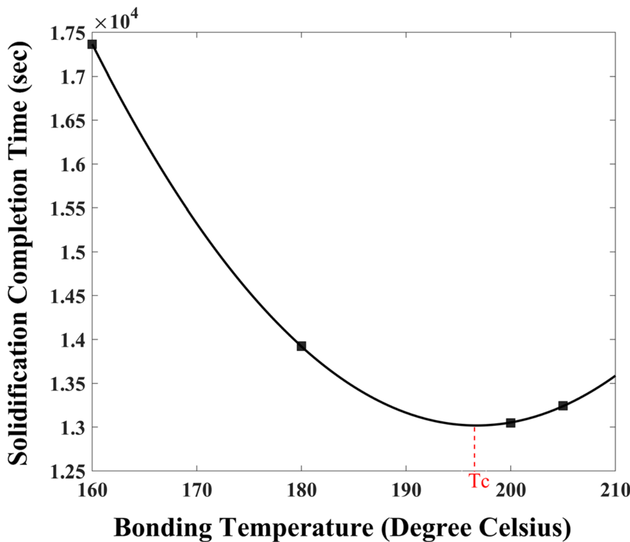

Fig. 13—Effect of increasing bonding temperature on bonding completion time t_f when TG is 5 °C/cm; gap size of 0.05 mm; and base-metal thickness of 1.0 mm.

D_s also influences the mode of solidification during the early stage of TG-TLP bonding process. In a situation where D_s is zero (ignored) the solidification mode is fully unidirectional starting from the beginning of

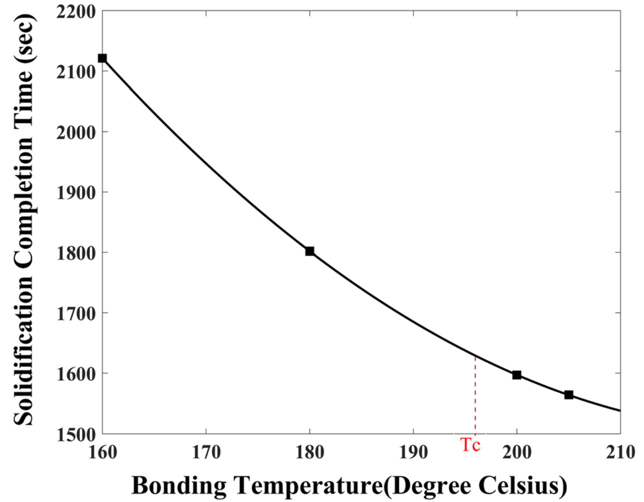

Fig. 14—Effect of increases in bonding temperature on bonding completion time t_f with a TG of 50 °C/cm; gap size of 0.05 mm; and base thickness of 1.0 mm.

solidification to the end (Figure 12). However, when a value of D_s is incorporated, at the beginning of the process, solidification occurs at the two solid–liquid interfaces to produce a bidirectional solidification, which later changes to unidirectional solidification as the process progresses (Figure 12). Bigvand[21] has experimentally observed the occurrence of bidirectional solidification at the early stage of TG-TLP bonding and this solidification model translated to unidirectional solidification mode at a later stage of the bonding process. This provides experimental validation of a key feature predicted by the numerical model developed and used in the present work. This thus shows that in contrast to what has been reported that solid-state diffusion can be ignored during the modeling of TG-TLP bonding, this work shows that solid state plays important roles during TG-TLP bonding, by reducing bonding completion time and influencing the mode of solidification, and, as such should not be ignored.

B. *Effect of Bonding Temperature Range During TG-TLP Bonding Process*

Most of the studies in the literature on the kinetics of TG-TLP bonding are focused on the impact of the magnitude of the temperature gradient; *i.e.*, how the magnitude of the TG affects the kinetics of solidification. However, at any given TG value, there can be several

temperature ranges, and the effect of temperature range on the kinetics of TG-TLP bonding has been hardly studied. In C-TLP bonding, temperature is known to have a significant effect on the solidification completion time t_f. A dual effect of an increase in temperature with solidification time has been observed.[22] The dual effect is a condition in which the t_f initially decreases as bonding temperature increases up to a critical temperature threshold of T_C, above which further increase in temperature increases the t_f, thus resulting in a U-shape curve when t_f *vs.* temperature is plotted.[22] In order to study the effect of temperature range during the TG-TLP bonding process on the occurrence of the dual temperature effect, a fixed TG value is used in the present work. The minimum temperature in each temperature range of the TG is used as a parameter to represent the temperature when plotting the solidification completion time against bonding temperature. The result presented in Figure 13 shows that the dual temperature effects are also possible during TG-TLP bonding. Generally, when temperature increases, the volume of liquid within the joint region increases and likewise the solidification kinetics increases. The decrease in t_f when the temperature is increased occurs when the extent of increase in the solidification kinetics is large enough to overcome the concomitant increase in the liquid volume. However, as the temperature is increased beyond a threshold temperature, T_C, the extent of increase in the solidification kinetics may not be large enough to overcome the attendant increase in the liquid volume and this would cause the t_f to increase as the temperature is increased. Further analysis shows that if the concentration gradient in the liquid, which is the key driving force that enhances solidification kinetics during TG-TLP bonding, is increased, the dual temperature effect can be prevented. A major bonding parameter that can be used to increase the concentration gradient in the liquid is the magnitude of the imposed TG. Figure 9 shows how the concentration gradient in the liquid at the solidifying solid–liquid interface varies with TG. By increasing the magnitude of the TG from 5 to 50 $^\circ$C/cm, the dual temperature effect is avoided as the solidification completion time monotonically reduces with increase in bonding temperature (Figure 14). Therefore, an undesirable increase in solidification completion time with increase in bonding temperature range can be avoided; adequate solute concentration gradient exists across the interlayer liquid phase during TG-TLP bonding.

IV. SUMMARY AND CONCLUSIONS

The key findings and conclusions in the work are summarized as follows:

1. A new TG-TLP bonding numerical model that incorporates variable diffusivity that not only changes with temperature but also with solute concentration in the solid has been developed and validated by experimental data reported in the literature.
2. A comparison of the solidification completion time between the C-TLP and TG-TLP bonding processes shows that instead of the high value of solute diffusivity in the liquid, the major reason why TG-TLP bonding produces shorter processing time compared to C-TLP bonding is due to the occurrence of solute concentration gradient in the liquid during TG-TLP bonding, which is essentially zero during C-TLP bonding.
3. Moreover, an increase in the solid-state diffusion coefficient is found to decrease the solidification completion time. This is attributable to the fact that solid-state diffusion plays a significant role of reducing the melting kinetics and increasing the solidification kinetics during the TG-TLP bonding process, notwithstanding the previous assumption in the literature that solid-state diffusion can be ignored during the modeling of TG-TLP bonding process.
4. Aside from affecting the kinetics of the bonding process, the result of an analysis performed by the new numerical model, which is validated by experimental result reported in the literature, shows that solid-state diffusion also influences the occurrence of bidirectional solidification mode at the early stage of the bonding process. The bidirectional solidification mode subsequently translates to unidirectional solidification as the TG-TLP bonding process progresses.
5. This study shows that a dual temperature effect, where solidification completion time decreases and later increases as bonding temperature is increased, can occur during TG-TLP bonding. However, this undesirable behavior can be avoided provided that the concentration gradient in the liquid is large enough to adequately enhance the solidification kinetics to persistently overcome the increased volume of liquid that accompanies increase in bonding temperature.

ACKNOWLEDGMENTS

The authors gratefully acknowledge financial support from the Natural Sciences and Engineering Research Council (NSERC) of Canada.

APPENDIX

The up/downwind approximations used in the analysis are

For positive velocity ($s^{n+1} > s^n$)		Negative velocity ($s^{n+1} < s^n$)	
$p^n_{j+1/2} = p^n_{j+1}$	$p^n_{j-1/2} = p^n_j$	$p^n_{j+1/2} = p^n_j$	$p^n_{j-1/2} = p^n_{j-1}$
$q^{n+1}_{j+1/2} = q^{n+1}_{j+1}$	$q^{n+1}_{j-1/2} = q^{n+1}_j$	$q^{n+1}_{j+1/2} = q^{n+1}_j$	$q^{n+1}_{j-1/2} = q^{n+1}_{j-1}$
$z^n_{j+1/2} = z^n_{j+1}$	$z^n_{j-1/2} = z^n_j$	$z^n_{j+1/2} = z^n_j$	$z^n_{j-1/2} = z^n_{j-1}$

Equation [8] is rearranged to calculate the future solute concentration, so that p_j^{n+1} gives Eq. (A1), where α_1, α_2 , and α_3 are the diffusion values obtained from the upwind solution. Separate values are derived for the downwind solution.

$$p_j^{n+1} = \alpha_1 p_j^n + \alpha_2 p_{j-1}^n + \alpha_3 p_{j+1}^n, \quad [A1]$$

$$\alpha_1 = \left(s1^n - \frac{\Delta t}{(\Delta u)^2} \frac{(D_A)_{j-1/2}^n + (D_A)_{j+1/2}^n}{s1^n} \right) / s1^{n+1} - \frac{(s1^{n+1} - s1^n) u_{j-1/2}}{\Delta u^e s1^{n+1}},$$

$$\alpha_2 = \left(\frac{\Delta t}{(\Delta u)^2} \frac{(D_A)_{j-\frac{1}{2}}^n}{s1^n} \right) / s1^{n+1},$$

$$\alpha_3 = \left(\frac{\Delta t}{(\Delta u)^2} \frac{(D_A)_{j+\frac{1}{2}}^n}{s1^n} \right) / s1^{n+1} + \frac{(s1^{n+1} - s1^n) u_{j+1/2}}{\Delta u^e s1^{n+1}}.$$

The future solute concentration of Phase C is derived by using similar approach, which is expressed in Eq. (A2), where γ_1, γ_2 , and γ_3 are the diffusion values obtained from the upwind solution. The values for the downwind solution are derived separately.

$$q_j^{n+1} = \gamma_1 q_j^{n-1} + \gamma_2 q_{j-1}^n + \gamma_3 q_{j+1}^n, \quad [A2]$$

$$\gamma_1 = \frac{(L - s2^{n-1}) - \frac{\Delta t}{(\Delta v)^2} \frac{(D_C)_{j-\frac{1}{2}}^n + (D_C)_{j+\frac{1}{2}}^n}{\{L - s2^n\}}}{(L - s2^{n+1})} - \frac{(s2^{n+1} - s2^n)(1 - v_{j-1/2})}{[\Delta u^e (L - s2^{n+1})]},$$

$$\gamma_2 = \left(\frac{\Delta t}{(\Delta v)^2} \frac{(D_C)_{j-\frac{1}{2}}^n}{(L - s2^n)(L - s2^{n+1})} \right),$$

$$\gamma_3 = \frac{\Delta t}{(\Delta v)^2} \frac{(D_C)_{j+\frac{1}{2}}^n}{(L - s2^n)(L - s2^{n+1})} + \frac{(s2^{n+1} - s2^n)(1 - v_{j+1/2})}{[\Delta u^e (L - s2^{n+1})]},$$

$$C_{BA}^n = \frac{1}{m}(T_0 - T_m) + \frac{G}{m} s1^n, \quad [A3]$$

$$C_{AB}^n = f \cdot C_{BA}^n, \quad [A4]$$

$$C_{BC}^n = \frac{1}{m}(T_0 - T_m) + \frac{G}{m} s2^n, \quad [A5]$$

$$C_{CB}^n = f \cdot C_{BC}^n. \quad [A6]$$

ABBREVIATIONS

TLP	Transient liquid phase
TG	Temperature gradient
C-TLP	Conventional transient liquid phase
TG-TLP	Temperature gradient transient liquid phase
D	Diffusion coefficient
MPD	Melting point depressant
$C(x,t)$	Concentration profile
$C_{AB} = C(s1(t)^-, t)$	Equilibrium concentration in Solid A
$C_{CB} = C(s2(t)^+, t)$	Equilibrium concentration in Solid C
$C_{BA} = C(s1(t)^+, t)$	Equilibrium concentration in Liquid/Solid A
$C_{BC} = C(s2(t)^-, t)$	Equilibrium concentration in Liquid/Solid B
$D(c(x,t))_{A,C}$	Diffusivity of Solid A or C
$p = p(u,t)$	Concentration profile of Solid A
$z = z(w,t)$	Concentration profile of liquid phase
$q = q(v,t)$	Concentration profile of Solid C
s1(t); s2(t)	Solid/Liquid Interfaces 1 and 2
λ	Geometric factor (0, 1 or 2 for planar, cylindrical or spherical geometry, respectively)
N, K, M	Number of discretizations in the phases
Q	Activation energy (kJ/mol)
R	Universal gas constant (kJ/mol K)
$G = dT/dX$	Temperature gradient across the bonding line
f	Partitioning coefficient between the liquidus and solidus lines
$m = dT/dC$	Slope of the temperature and solute composition
T_m	Melting temperature of a material
T_o	Lowest bonding temperature on temperature gradient line

REFERENCES

1. A.A. Shirzadi and E.R. Wallach: *Acta Mater.*, 1999, vol. 47, pp. 3551–60.
2. T.M. Pollock and S. Tin: *J. Propuls. Power*, 2006, vol. 22, pp. 361–74.
3. M. Liu, G. Sheng, H. He, and Y. Jiao: *J. Mater. Process. Technol.*, 2017, vol. 246, pp. 245–51.
4. W.F. Gale: *JOM*, 1999, vol. 51, pp. 49–52.
5. Y. Zhou, W.F. Gale, and T.H. North: *Int. Mater. Rev.*, 1995, vol. 40, pp. 181–96.
6. I. Tuah-Poku, M. Dollar, and T.B. Massalski: *Metall. Trans. A*, 1988, vol. 19, pp. 675–86.
7. W.D. MacDonald and T.W. Eagar: *Annu. Rev. Mater. Sci.*, 1992, vol. 22, pp. 23–46.
8. D.S. Duvall, W.A. Owczarski, and D.F. Paulonis: *Weld. J. (Miami Fla.)*, 1974, vol. 53, pp. 203–14.

9. T.L. Yang, T. Aoki, K. Matsumoto, K. Toriyama, A. Horibe, H. Mori, Y. Orii, J.Y. Wu, and C.R. Kao: *Acta Mater*., 2016, vol. 113, pp. 90–97.
10. M.A. Jabbareh and H. Assadi: *Scripta Mater*., 2009, vol. 60, pp. 780–82.
11. H. Assadi, A.A. Shirzadi, and E.R. Wallach: *Acta Mater*., 2001, vol. 49, pp. 31–39.
12. T.C. Illingworth, I.O. Golosnoy, V. Gergely, and T.W. Clyne: *J. Mater*. *Sci*., 2005, vol. 40, pp. 2505–11.
13. A. Ghanbar, D.E. Michael, and O.A. Ojo: *Philos*. *Mag*., 2019, vol. 99, pp. 2169–84.
14. J. Crank: *Free and Moving Boundary Problems*, Clarendon Press, Oxford, 1984.
15. A. Ghanbar: MSc Thesis, University of Manitoba, 2019.
16. M. Rappaz, M. Bellet, and M. Deville: *Numerical Modeling in Materials Science and Engineering, Springer Series in Computational Mathematics*, Springer, Berlin, 2003.
17. N. Yamada, S. Suzuki, and K. Suzuki: *Int*. *J*. *Microgravity Sci*. *Appl*., 2019, vol. 35, p. 350402.
18. A.M. Delhaise and D.D. Perovic: *J*. *Electron*. *Mater*., 2018, vol. 47, pp. 2057–65.
19. Y. Zhong, N. Zhao, H.T. Ma, W. Dong, M.L. Huang, and C.P. Wong: *Proc*. *Electron*. *Compon*. *Technol*. *Conf*., 2017, pp. 411–16.
20. Z. Yin, F. Sun, and M. Guo: *J*. *Mater*. *Sci*. *Mater*. *Electron*., 2019, vol. 30, pp. 2146–53.
21. A.G. Bigvand: MSc Thesis, University of Manitoba, 2013.
22. M.M. Abdelfatah and O.A. Ojo: *Metall*. *Mater*. *Trans*. *A*, 2009, vol. 40A, pp. 377–85.

Publisher's Note Springer Nature remains neutral with regard to jurisdictional claims in published maps and institutional affiliations.